Available online at www.sciencedirect.com
ScienceDirect
Journal of Sound and Vibration 318 (2008) 1119–1138
JOURNAL OF SOUND AND VIBRATION
www.elsevier.com/locate/jsvi

Stability of synchronized network of chaotic electromechanical devices with nearest and all-to-all couplings

G.S. Mbouna Ngueuteu[a], R. Yamapi[b,*], P. Woafo[a]

[a]*Laboratory of Modelling and Simulation in Engineering and Biological Physics, Faculty of Science, University of Yaoundé I, Box 812, Yaoundé, Cameroon*
[b]*Department of Physics, Faculty of Science, University of Douala, Box 24, 157 Douala, Cameroon*

Received 26 November 2007; received in revised form 16 April 2008; accepted 22 April 2008
Handling Editor: C.L. Morfey
Available online 10 June 2008

Abstract

A shift-invariant set of N mutually (nearest-neighbour or all-to-all) coupled moving coil electromechanical devices is analytically and numerically investigated. The study of the stability of synchronization process is undertaken using the master stability function (MSF) approach. The emanating properties of this method make it possible to have a general study of the network dynamics, and to explain de-synchronization phenomena appearing in the synchronization stability parametric areas. A detailed attention is paid to the effects of the dissipative component of the dispersive–dissipative coupling tested here.

1. Introduction

In recent years, the importance of the concept of collective and self-organized behaviour has been recognized in many different areas of science. Complex networks have provided a challenging framework for the study of synchronization of dynamical units, based on the interplay between complexity in the overall topology and local dynamical properties of the coupled units. In particular, the effects of synchronization in systems of coupled oscillators nowadays provide a unifying framework for different phenomena observed in nature [1,2]. In the study of synchronization, it is important to determine conditions for the stability of the synchronous behaviour for a generic network topology with a generic coupling configuration. Consequently, increasingly powerful mathematical methods are being developed to seek the potential conditions for realization of the most interesting form of dynamical behaviour that can arise in these networks: synchronization. These methods reverse the question by studying when a synchronous state is stable, in terms of coupling scheme and especially of coupling strengths. The master stability function (MSF) approach has been introduced to address this question for arrays of coupled oscillators [3]. This method has been later extended to the case of complex networks of dynamical systems coupled with arbitrary topologies like those in Refs. [4–10].

*Corresponding author. Tel: +237 99 32 93 76; fax: +237 340 75 69.
E-mail addresses: ngueut@yahoo.fr (G.S. Mbouna Ngueuteu), ryamapi@yahoo.fr (R. Yamapi), pwoafo1@yahoo.fr (P. Woafo).

0022-460X/$ - see front matter
doi:10.1016/j.jsv.2008.04.051

Researches in the fields of collective dynamics and spatiotemporal dynamics have been a subject of particular interest. This is due to their importance in many scientific fields, ranging from electronics and telecommunication [3,7,9,11–22], electromechanical engineering [22–25], physics [20,26–28], chemistry [29,30], biology [10,16,17,21,22] to social sciences (see Refs. [1,2] for more information on applications of synchronization phenomena).

The present paper considers the stability of a synchronized network of N chaotic electromechanical devices, coupled through a linear capacitor and resistance, connected in series. Each electromechanical system consists of a Duffing-quintic electrical oscillator coupled magnetically to the linear mechanical oscillator. Our aim is to find how the topology and local dynamical properties of the coupled units can affect the synchronization process. Moreover, the stability of synchronization process will be carried out following the MSF approach [2–7,9,11] based on the variations (varying to some parameters, such as number of subsystems or coupling strengths) of the largest transverse Lyapunov exponent. The MSF approach makes it possible to derive the coupling strengths ranges, leading to stable synchronous states in the network of coupled chaotic electromechanical devices. This method also makes it possible to explain the emergence of some instability such as bursting and cluster patterns, and other de-synchronization phenomena [3].

The paper is organized as follows. In the next section, we describe the shift-invariant set of N mutually coupled electromechanical devices under nearest-neighbour coupling and all-to-all coupling configurations. After this, we review the chaotic dynamical behaviour found recently in Ref. [24] by presenting the range of amplitude of the external excitation enabling us to deduce the conditions of emergence of chaos in the dynamics of an electromechanical device. Section 3 tackles the analytical investigation of the stability of synchronization states in the network under nearest-neighbour coupling and all-to-all coupling configurations. Detailed attention is paid to the effect of the dissipative component of the coupling (the resistance) on the stability of the synchronization process. Section 4 deals with computation of the MSF through the numerical simulations. The transition boundaries between the stable and unstable synchronization are found and several different dynamical states are derived. We end the paper with conclusions drawn from this work.

2. Description of the physical system and chaotic behaviour

We consider a network of N identical electromechanical devices, mutually coupled to each other by their electrical parts through the series-association of a capacitor and a resistance (dispersive–dissipative coupling). The network is considered with two connectivity configurations: the nearest-neighbour coupling configuration and the all-to-all coupling configuration shown, respectively in Figs. 1 and 2 (in Fig. 2, we limit ourselves to four nodes for visibility reasons). Each electromechanical system presented in Fig. 3 is made of a linear mechanical oscillator coupled to a Duffing-quintic electrical oscillator. The interaction between these two parts is ensured by a uniform magnetic flux of density B produced by a permanent magnet (see Ref. [24] for more information). The mechanical part is made up of a mobile beam with mass m that can oscillate along the z-axis. The operating rod is bound to the mobile beam and is enclosed in a spring of stiffness coefficient k.

According to the second Newton law of dynamics, the mechanical part of each electromechanical device is described by

$$m\ddot{z}_i + \lambda\dot{z}_i + kz_i - lB\dot{q}_i = 0, \quad i = 1, 2, \ldots, N, \tag{1}$$

where λ is the viscous friction coefficient and l the length of the moving coil. The electrical part consists of a resistance R, a nonlinear capacitor C (which provides the Duffing-quintic nonlinearity via its voltage–charge characteristic: $V_{C,i}(q_i) = (1/C_0)(q_i + a_3q_i^3 + a_5q_i^5)$, and an inductor L, all connected in series with a sinusoidal voltage source $e(\tau) = v_0 \cos\Omega\tau$ (where τ is the time, v_0 the amplitude and Ω the frequency).

Let V_i be the voltage of the ith electromechanical system, directed every time in the contrary direction of the current I_i through this electromechanical device, V_{ij} the voltage of the branch coupling between the ith and jth systems, I_{ij} the current crossing this branch, and q_{ij} be the coupling capacitor charge. Then,

$$V_i = L\ddot{q}_i + R\dot{q}_i + \frac{1}{C_0}q_i + a_3q_i^3 + a_5q_i^5 + lB\dot{z}_i - v_0\cos\Omega\tau. \tag{2}$$

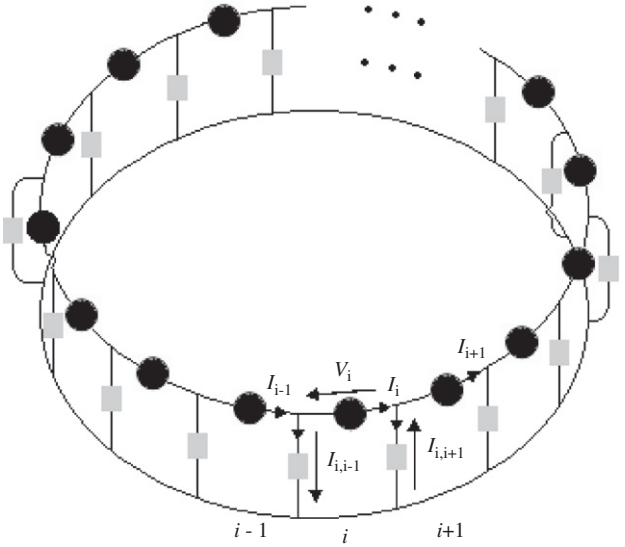

Fig. 1. The schema of the nearest-neighbour mutually coupled electromechanical systems.

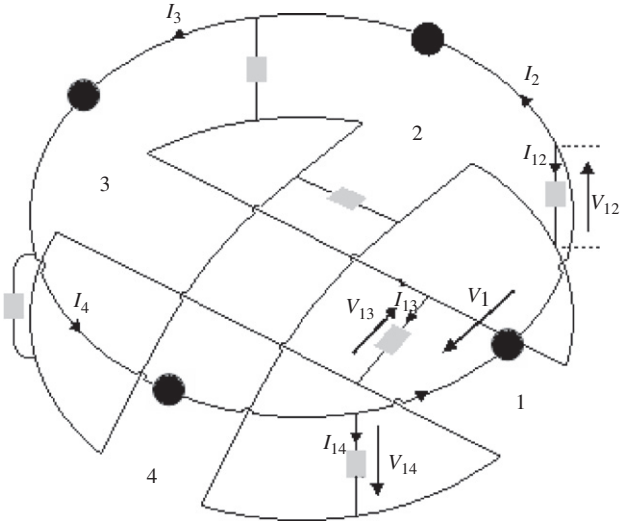

Fig. 2. The schema of the all-to-all mutually coupled electromechanical systems.

Before continuing this analysis, let us mention that the expression of the voltage V_i depends on the type of coupling configuration. We will now consider separately the two types of coupling configuration and determine the differential equations of motion in each case.

2.1. The nearest-neighbour coupling configuration

In the case of diffusive coupling configuration, the Kirchhoff's voltage and current laws imply that the electrical signals in the ith electromechanical device presented in Fig. 1 are determined by

$$V_i = -V_{i,i-1} - V_{i,i+1}, \tag{3}$$

$$I_{i,i-1} = -I_{i-1,i} = I_i - I_{i-1} \text{ and } I_{i,i+1} = I_i - I_{i+1}. \tag{4}$$

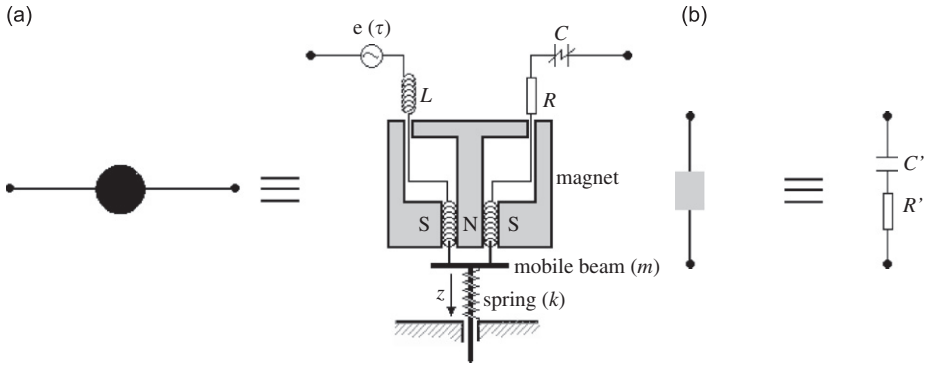

Fig. 3. (a) Each electromechanical moving coil transducer and (b) each coupling elements link.

Now, according to Eq. (4), as a general rule,

$$V_{ij} = \frac{1}{C'} q_{ij} + R' I_{ij} = \frac{1}{C'}(q_i - q_j) + R'(I_i - I_j). \tag{5}$$

Substituting Eq. (5) into Eq. (3) yields the following equation:

$$V_i = \frac{1}{C'}(q_{i-1} - q_i) + R'(\dot{q}_{i-1} - \dot{q}_i) - \frac{1}{C'}(q_i - q_{i+1}) - R'(\dot{q}_i - \dot{q}_{i+1}). \tag{6}$$

The differential equation (2) enables us to derive the following equation describing the electrical part of each electromechanical device of the network

$$L\ddot{q}_i + R\dot{q}_i + \frac{1}{C_0} q_i + a_3 q_i^3 + a_5 q_i^5 + lB\dot{z}_i - v_0 \cos \Omega\tau = \frac{1}{C'}(q_{i-1} - 2q_i + q_{i+1}) + R'(\dot{q}_{i-1} - 2\dot{q}_i + \dot{q}_{i+1}),$$
$$i = 1, 2, \ldots, N. \tag{7}$$

Therefore, the shift-invariant set of N nearest-neighbour coupled electromechanical devices is described by

$$\begin{gathered} L\ddot{q}_i + R\dot{q}_i + \tfrac{1}{C_0} q_i + a_3 q_i^3 + a_5 q_i^5 + lB\dot{z}_i - v_0 \cos \Omega\tau = \tfrac{1}{C'}(q_{i-1} - 2q_i + q_{i+1}) + R'(\dot{q}_{i-1} - 2\dot{q}_i + \dot{q}_{i+1}), \\ m\ddot{z}_i + \lambda\dot{z}_i + kz_i - lB\dot{q}_i = 0, \qquad i = 1, 2, \ldots, N. \end{gathered} \tag{8}$$

Define the dimensionless variables $x_i = q_i/Q_0$, $y_i = z_i/l$, $t = \omega_e\tau$, where $\omega_e = 1/\sqrt{LC_0}$ and Q_0 is the reference charge of the capacitor. Then Eq. (8) yield the following set of coupled non-dimensional equations:

$$\ddot{x}_i + \gamma_1\dot{x}_i + x_i + \beta_1 x_i^3 + \beta_2 x_i^5 + \lambda_1\dot{y}_i - E_0 \cos \omega t = K_1(x_{i-1} - 2x_i + x_{i+1}) + K_2(\dot{x}_{i-1} - 2\dot{x}_i + \dot{x}_{i+1}),$$
$$\ddot{y}_i + \gamma_2\dot{y}_i + \omega_2^2 y_i - \lambda_2\dot{x}_i = 0, \qquad i = 1, 2, \ldots, N \tag{9}$$

with

$$\gamma_1 = \frac{R}{L\omega_e},\ \beta_1 = \frac{a_3 Q_0^2}{L\omega_e^2},\ \beta_2 = \frac{a_5 Q_0^4}{L\omega_e^2},\ \lambda_1 = \frac{l^2 B}{LQ_0\omega_e},\ \gamma_2 = \frac{\lambda}{m\omega_e},$$
$$\omega_2^2 = \frac{k}{m}\frac{1}{\omega_e^2},\ \lambda_2 = \frac{BQ_0}{m\omega_e},\ E_0 = \frac{v_0}{LQ_0\omega_e},\ K_1 = \frac{C_0}{C'},\ K_2 = \frac{R'}{L\omega_e},\ w = \frac{\Omega}{\omega_e}.$$

The variables K_1 and K_2 are, respectively, the capacitive and resistive coupling coefficients. The network of electromechanical devices with nearest-neighbour coupling configuration is described by a system of N coupled differential equations consisting of an electrical Duffing-quintic oscillator coupled magnetically to the linear mechanical oscillator.

2.2. The all-to-all coupling configuration

In the case of all-to-all coupling configuration, Kirchhoff's voltage law, applied to the ith electromechanical device, establishes the following equation:

$$V_i + V_{i1} + V_{i2} + \cdots + V_{iN} = 0, \tag{10}$$

where $V_{ij} = (1/C')q_{ij} + R'I_{ij}$. It appears that the relation between currents and charges obtained through the application of Kirchhoff's current law to all the nodes of the circuit is complex when the number of electromechanical devices is large. Because of the complexity of the resulting relations, we chose to establish equations for the first oscillator in the set of four coupled electromechanical devices (see Fig. 2). We note that we do not lose generality by choosing oscillator 1 in a network of four electromechanical devices, since a conjecture and a circular rotation would enable us to obtain the equation describing any unit i in the network of N electromechanical devices. A rather obvious handling of Kirchhoff's current law shows that $I_{1j} = I_1 - I_j$, and therefore, $q_{1j} = q_1 - q_j$. In this case, Eq. (10) yields

$$V_1 = \frac{1}{C'}\sum_{j=2}^{4}(q_j - q_1) + R'\sum_{j=2}^{4}(\dot{q}_j - \dot{q}_1). \tag{11}$$

The circular rotation and the conjecture lead to the following relation:

$$V_i = \frac{1}{C'}\sum_{j=1, j\neq i}^{N}(q_j - q_i) + R'\sum_{j=1, j\neq i}^{N}(\dot{q}_j - \dot{q}_i). \tag{12}$$

Eqs. (2) and (12) lead to the following equation describing the electrical part of each electromechanical device of the network:

$$L\ddot{q}_i + R\dot{q}_i + \frac{1}{C_0}q_i + a_3q_i^3 + a_5q_i^5 + lB\dot{z}_i - v_0\cos\Omega\tau = \frac{1}{C'}\sum_{j=1, j\neq i}^{N}(q_j - q_i) + R'\sum_{j=1, j\neq i}^{N}(\dot{q}_j - \dot{q}_i), \quad i = 1, 2, \ldots, N.$$

Therefore, the shift-invariant set of N all-to-all coupled Duffing-quintic electromechanical devices is described by

$$\begin{aligned} &L\ddot{q}_i + R\dot{q}_i + \frac{1}{C_0}q_i + a_3q_i^3 + a_5q_i^5 + lB\dot{z}_i - v_0\cos\Omega\tau = \frac{1}{C'}\sum_{j=1, j\neq i}^{N}(q_j - q_i) + R'\sum_{j=1, j\neq i}^{N}(\dot{q}_j - \dot{q}_i),\\ &m\ddot{z}_i + \lambda\dot{z}_i + kz_i - lB\dot{q}_i = 0, \quad i = 1, 2, \ldots, N. \end{aligned} \tag{13}$$

Eq. (13) can be rewritten to the following set of coupled non-dimensional equations:

$$\begin{aligned} &\ddot{x}_i + \gamma_1\dot{x}_i + x_i + \beta_1x_i^3 + \beta_2x_i^5 + \lambda_1\dot{y}_i - E_0\cos\omega t = Q_1\sum_{j=1, j\neq i}^{N}(x_j - x_i) + Q_2\sum_{j=1, j\neq i}^{N}(\dot{x}_j - \dot{x}_i),\\ &\ddot{y}_i + \gamma_2\dot{y}_i + \omega_2^2y_i - \lambda_2\dot{x}_i = 0, \quad i = 1, 2, \ldots, N, \end{aligned} \tag{14}$$

where $Q_1 = C_0/C'$, $Q_2 = R'/L\omega_e$.

The interest devoted to these systems is due to their possible applications in electromechanical engineering and the construction of various vibro-technical devices both at the microscopic and macroscopic levels. As we have recently observed in Ref. [24], each electromechanical model is widely encountered in various branches of electromechanical engineering. For some technological exploitation of such device, it is interesting (for engineering purposes) to use many identical electromechanical devices coupled mutually as shown in Figs. 1 and 2. In industry, these synchronized networks of electromechanical devices operate in parallel mode for common loading in assembly line works and in manufacturing processes: i.e a series of perforation devices or a series of macro/micro-electromechanical devices uses for cutting, drilling and other machining work. The

chaotic state is particularly of interest when the network of mutually coupled chaotic electromechanical systems is used for industrial operations such as the mixing of different liquids, chemicals or powders. Moreover, one can also connect the operating rods of the synchronized transducers network to a yielding membrane to make a vibrating membrane. Such a system (transducers network plus membrane) can be exploited in pneumatic systems. On the microscopic scale it can be used for the design of certain artificial organs. By varying the coupling coefficients K_i and Q_i, one can obtain various dynamical states such as clusters, complete synchronization and even instability. In the complete synchronization state, all the rods T of the mechanical oscillators vibrate in phase.

2.3. Chaotic behaviour in the uncoupled electromechanical unit

We find in this subsection how chaos arises in the electromechanical model as the parameters of the system vary. For this purpose, we numerically solve the equations of motion without coupling ($K_1 = K_2 = Q_1 = Q_2 = 0$) and plot the resulting bifurcation diagrams as E_0 varies. The following transitions are observed through the bifurcation diagram presented in Fig. 4(a). When E_0 increases from 0, the system presents a period-T orbit until $E_0 = 24.72$, where a series of period doubling cascade appears and lead to a band of chaotic movement at $E_0 = 27.05$. Around this value, there is a small interval of E_0 where multi-periodic, quasi-periodic and chaotic behaviours are intermingled. As E_0 increases further, there is a break of chaotic movement at $E_0 = 30.04$, the system rearranges itself in $3T$-period orbits and the chaotic movement

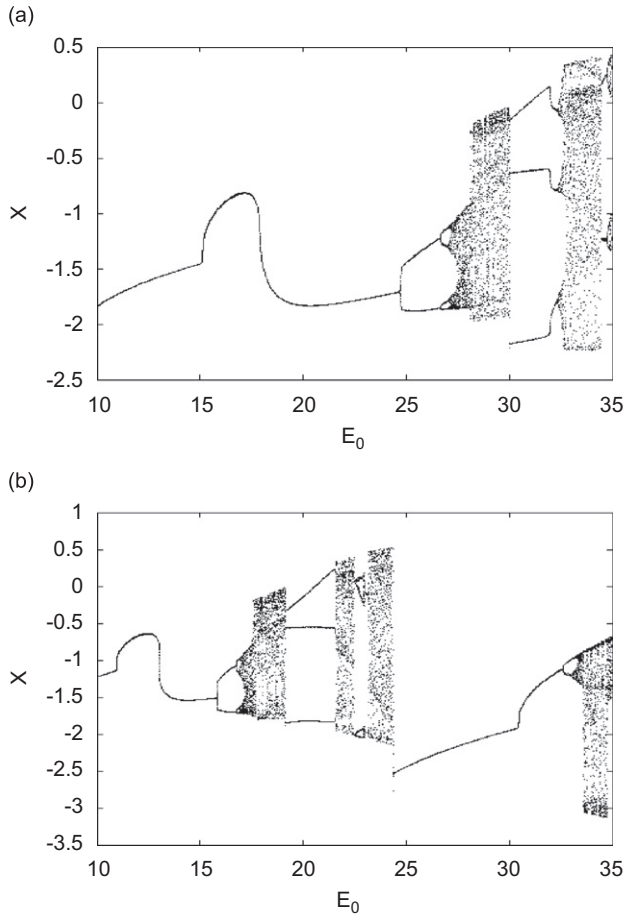

Fig. 4. Bifurcations diagrams versus the amplitude E_0 of the external excitation. (a) $\beta_2 = 0$ and (b) $\beta_2 = 0.1$ and the other parameters are $\gamma_1 = 0.2$, $\gamma_2 = 0.1$, $\lambda_1 = 0.01$, $\lambda_2 = 0.05$, $\omega_2 = 1.2$, $\omega = 0.85$, $\beta_1 = 0.9$.

returns at $E_0 = 32.55$. Analysing the effects of higher nonlinearity, one finds in Fig. 4(b) that the quintic nonlinearity compresses the bifurcations tree. This implies an early appearance of nonlinear phenomena (chaos for instance) as E_0 increases [24].

3. Stability of synchronization in the network

This section deals with the stability of the synchronization process in a network of mutually coupled chaotic electromechanical systems. This model is only of interest if the resulting dynamical state is stable. This requires that each of the perturbed trajectories returns to its original attractor. This investigation will enable us to identify various dynamical states which appear in the network, depending on the coupling strength K_1, K_2, Q_1, Q_2 and the number N of chaotic electromechanical systems. In order to rewrite Eq. (14) as a system of flows, we introduce new variables $u_v = \dot{x}_v$, $v_v = \dot{y}_v$ to obtain the following set of first-order differential equations:

$$\begin{aligned}
&\dot{x}_v = u_v,\\
&\dot{u}_v = E_0 \cos wt - \gamma_1 u_v - x_v - \beta_1 x_v^3 - \beta_2 x_v^5 - \lambda_1 v_v, \quad v = 1, 2, \ldots, N\\
&\dot{y}_v = v_v,\\
&\dot{v}_v = -\gamma_2 v_v - w_2^2 y_v + \lambda_2 u_v.
\end{aligned}$$

When the electromechanical oscillators are coupled, the resulting dynamical state of the system is interesting when it lies within the synchronization manifold S defined by $(x_1, u_1, y_1, v_1) = (x_2, u_2, y_2, v_2) = \cdots = (x_N, u_N, y_N, v_N) = (x_s, u_s, y_s, v_s)$. The stability of such a synchronization manifold S will be the main purpose of the study. Our investigation will make use of the MSF approach [2,3]. Therefore, we will next derive the variational problem giving rise to the MSF approach, which provides a stability condition for the hyper surface S. Eqs. (9) and (14) can be rewritten in the following single vector form:

$$\dot{X}_i = \mathbf{F}(X_i, t) + \sum_{j=1}^{N} G_{ij}\mathbf{H}(X_j), \tag{15}$$

where $X_i = (x_i, u_i, y_i, v_i)^{\mathrm{T}}$ is the quadri-vector of the dynamical variables of the ith electromechanical system, the function $\mathbf{F} : \mathbb{R}^4 \to \mathbb{R}^4$ describes the local dynamics of the ith system, and the function $\mathbf{H} : \mathbb{R}^4 \to \mathbb{R}^4$ carrying the coupling strengths, describes the coupling between these chaotic electromechanical systems. The functions $\mathbf{F}$ and $\mathbf{H}$ are defined by the equations:

$$\mathbf{F}(X_i, t) = \begin{pmatrix} u_i \\ E_0 \cos \omega t - \gamma_1 u_i - x_i - \beta_1 x_i^3 - \beta_2 x_i^5 - \lambda_1 v_i \\ v_i \\ -\gamma_2 v_i - \omega_2^2 y_i + \lambda_2 u_i \end{pmatrix} \text{and } \mathbf{H}(X_i) = \mathbf{E}.X_i.$$

Finally, G_{ij} are the components of the $N \times N$ symmetrical connectivity matrices $\mathbf{G}$, relative to the considered coupling scheme:

- In the case of nearest-neighbour coupling configuration, the coupling matrix $\mathbf{G}$ and $\mathbf{E}$ are:

$$\mathbf{G} = \begin{pmatrix} -2 & 1 & 0 & \ldots & 1 \\ 1 & -2 & 1 & \ddots & 0 \\ 0 & \ddots & \ddots & \ddots & \vdots \\ \vdots & \ddots & \ddots & \ddots & 1 \\ 1 & 0 & \ldots & 1 & -2 \end{pmatrix} \text{ and } \mathbf{E} = \begin{pmatrix} 0 & 0 & 0 & 0 \\ K_1 & K_2 & 0 & 0 \\ 0 & 0 & 0 & 0 \\ 0 & 0 & 0 & 0 \end{pmatrix}.$$

- While for the case of all-to-all coupling configuration, we have

$$\mathbf{G}=\begin{pmatrix} -N+1 & 1 & \dots & 1 \\ 1 & \ddots & \ddots & \vdots \\ \vdots & \ddots & \ddots & 1 \\ 1 & \dots & 1 & -N+1 \end{pmatrix} \text{ and } \mathbf{E}=\begin{pmatrix} 0 & 0 & 0 & 0 \\ Q_1 & Q_2 & 0 & 0 \\ 0 & 0 & 0 & 0 \\ 0 & 0 & 0 & 0 \end{pmatrix}.$$

Due to the zero row-sum condition of the coupling matrix ($\sum_j G_{ij}=0, \forall i$) and to the fact that the function $\mathbf{H}(X_i)$ is the same for all shift-invariant network units, the synchronization manifold S is an invariant set. These two properties guarantee that the coupling term of Eq. (15) vanishes exactly on S. Therefore, stability of the synchronous state reduces to taking care of the system's dynamical properties along directions in phase's space that are transverse to the synchronization manifold.

The stability of the synchronization state in the network can be studied through the linearization of Eq. (15) around the synchronous state $X_s=(x_s,u_s,y_s,v_s)^{\mathrm{T}}$ according to

$$\dot{\varepsilon}_i = D\mathbf{F}(X_s)\varepsilon_i + \sum_{j=1}^{N} G_{ij} D\mathbf{H}(X_s)\varepsilon_j, \tag{16}$$

where ε_i is the deviation of X_i from the synchronization manifold. We recall that γ_i and ϖ_i are the set of real eigenvalues and the associated orthonormal eigenvectors of the matrix $\mathbf{G}$, respectively, so that $\mathbf{G}\varpi_i=\gamma_i\varpi_i$ and $\varpi_i^{\mathrm{T}}\varpi_j=\delta_{ij}$. The arbitrary state ε_k can be written as $\varepsilon_k=\sum_{k=0}^{N-1}\varpi_k\otimes\eta_k(t)$, with $\eta_k(t)=\left(\eta_k^1(t),\ \eta_k^2(t),\ \eta_k^3(t),\ \eta_k^4(t)\right)$. If one applies ϖ_j^{T} to the left-hand side of each equation of systems (16), one finally obtains the following set of N variational equations:

$$\dot{\eta}_k = [D\mathbf{F}(X_s)+\gamma_k\mathbf{E}]\eta_k, \quad k=0,1,2,\dots,N-1. \tag{17}$$

We recall that γ_k is the eigenvalue of $\mathbf{G}$, and is given by $\gamma_k=-4\sin^2(k\pi/N)$ for the nearest-neighbour coupling [3] and $\gamma_0=0$, $\gamma_k=-N$ ($k\neq0$) for the all-to-all or global coupling [4].

As it appears in the literature [11], each Eq. (17) corresponds to a set of 4 conditional Lyapunov exponents $\lambda_k^j(j=1,\dots,4)$, along the eigenmode corresponding to the eigenvalue γ_k. Moreover, because of the degeneracy of $\mathbf{G}$'s eigenmodes spectrum, Eq. (17) leads to a set of $4\times\mathrm{int}(N/2)$ (respectively 4×1) conditional Lyapunov exponents in the case of nearest-neighbour coupling (respectively in the case of all-to-all coupling), along all the transverse eigenmodes. Here int(.) stands for the integer part function. This degeneracy of $\mathbf{G}$'s spectrum reduces the problem of the resolution of Eq. (17) to a more handy low-dimensional system, which helps make computation of the transverse Lyapunov exponents fast. As it appears in the literature, a necessary condition for stability of the synchronization manifold is that the set of conditional Lyapunov exponents is entirely made up of negative values [3].

Whatever the considered coupling scheme, $\mathbf{G}$'s spectrum contains the eigenvalue $\gamma_0=0$ corresponding to the eigenmode lying entirely within S. For this reason the eigenmode $k=0$ is described as longitudinal. This implies that the stability of synchronous states is reduced to the dynamical properties of the coupled electromechanical systems along the trajectories transverse to S. The transverse modes ($k\neq0$) describe the system response to a perturbation around S, so that, they consequently provide a framework for the study of the stability of synchronization. In addition, any deviation from S, however tiny it may be, is characterized by the growth of at least one transverse Lyapunov exponent.

The parametric behaviour (depending on N, K_1 and K_2, or Q_1 and Q_2 values) of the maximum of such exponents, called the MSF Λ, gives information about the general dynamics of the network. Why do Λ's variations seem as significant as its sign? In fact, the stability criteria used in the past (negativity of the sub-Lyapunov exponents [12], Floquet theory [14–17,21,23]) do not guarantee the non-existence of unstable invariants sets in the synchronous states or locally unstable areas on the attractor, which both, cause some de-synchronization phenomena. Nevertheless, the universal stability standard $\Lambda<0$, implies that any deviation from S should decay and vanish as time goes on. Knowing that Eq. (17) merge into those of an uncoupled electromechanical device for the longitudinal mode (i.e. $K_1=K_2=0$ or $Q_1=Q_2=0$), it is clear that the hyper

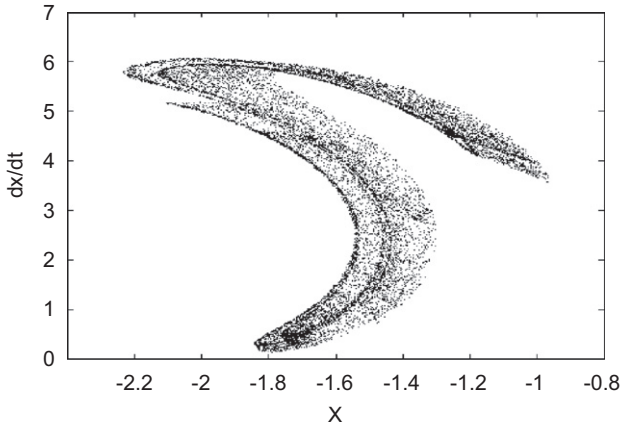

Fig. 5. The Poincaré cross section in the space $\{x(t), \dot{x}(t)\}$ with the parameters: $\beta_2 = 0.1$, $E_0 = 18.4$ and those of Fig. 4.

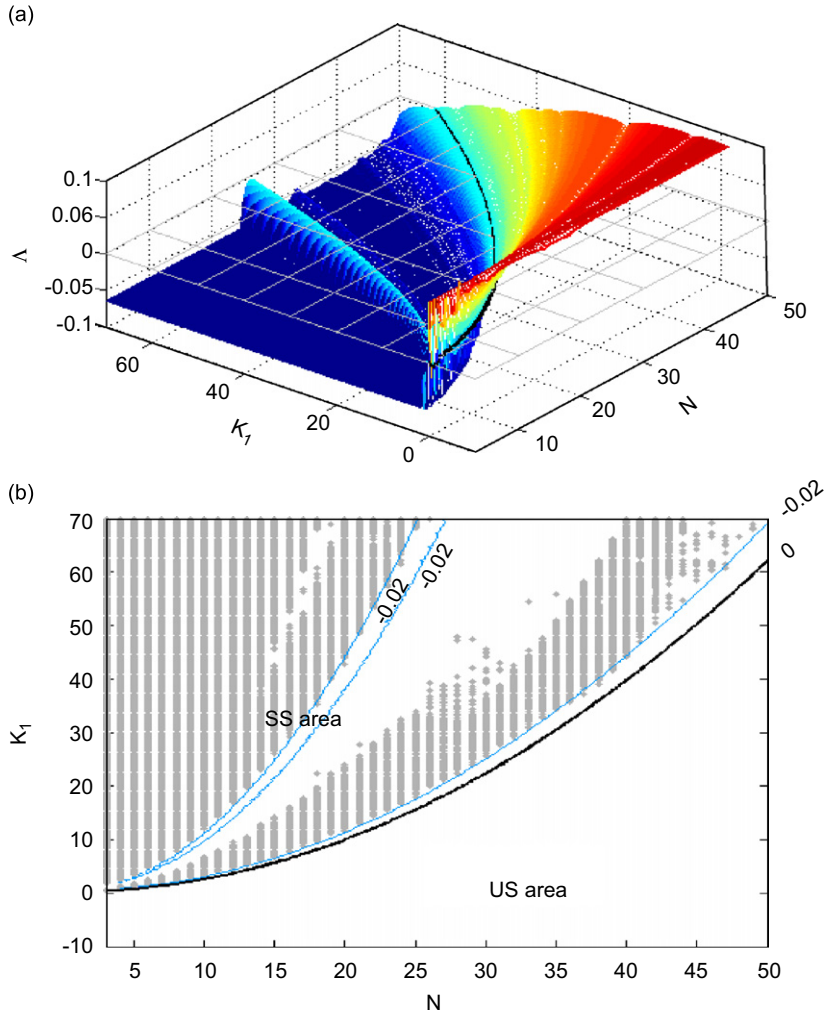

Fig. 6. (a) The MSF in the parametric plane (N, K_1): the region of stable synchronization is the region under the plane $\Lambda = 0$ displayed by the grid and the solid line is the stability threshold. (b) The corresponding stability map: (——) stability threshold $\Lambda = 0$; the other lines are Λ's contours; the dark domain is the complete synchronization area (obtained numerically). For $K_2 = 0$ and the other parameters are those of Fig. 5.

surface S will be a chaotic attractor (of which one of the Poincaré cross sections is represented in Fig. 5) and consequently $\lambda_0^{\max} > 0$. We must recall that when the coupling is turned off ($K_1 = K_2 = Q_1 = Q_2 = 0$), all the transverse modes degenerate into the longitudinal one, but also note, however, that this does not mean that the transverse modes lay within S, owing to the fact that a set of uncoupled chaotic units cannot synchronize.

4. Numerical simulations and results

We focus on the numerical computation of the MSF, by solving the equations of motion and the associated variational equations using the fourth-order Runge–Kutta algorithm. This MSF will help us to find various dynamical states and to establish some stability maps in the (N, K_1), (K_1, K_2), (N, Q_1) and (Q_1, Q_2) parametric planes, which will in turn provide the dynamical behaviour of the network, depending on the coupling parameters.

Direct numerical simulations of Eqs. (9) and (14) for the network of chaotic electromechanical systems, launched in rather close points of the phases space, confirm the results shown on these maps. Numerically, we suppose that complete synchronization is achieved in the network after a certain time t_{syn}, known as the synchronization time, after which one of the following criteria is verified:

$$\frac{|x_i(t) - x_j(t)|}{(N-1)^2} < h, \quad \forall (i,j) \text{ and } \forall t > t_{\text{syn}}, \tag{18}$$

$$\frac{\sum_{i=1}^{N} x_i(t) - x_{i+1}(t)}{(N-1)^2} < h, \quad \forall t > t_{\text{syn}} \text{ with } x_{N+1} = x_1, \tag{19}$$

where $h = 10^{-3}$ is the synchronization precision. These two criteria lead to the same result.

4.1. The nearest-neighbour coupling configuration

4.1.1. Dispersive coupling case, i.e. $K_2 = 0$

Before carried out this discussion on the boundary for stable synchronization onset in $\boldsymbol{K}_1$ and N parameter space, we note that the boundary appears quadratic in N. This might be explained by noting that the eigenvalues for the system are $\gamma_k = -4K_1 \sin^2(k\pi/N)$ and that the mode with the smallest eigenvalue ($k = 1$) will be the last to cross the threshold. Approximating the sine function by its argument we have $\gamma_1 = -4K_1(\pi/N)^2$. Thus, the boundary is given by the line for which the coupling times the eigenvalue is the zero of the MSF Λ, and we have, $\Lambda = \lambda_1 = 0 \Rightarrow -4K_1(\pi/N)^2 = \text{const} \Rightarrow K_1 \cong (N/\pi)^2$, a quadratic function.

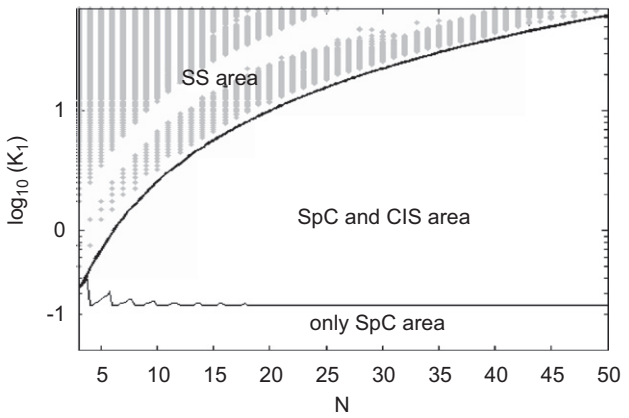

Fig. 7. The stability map of Fig. 6 in the semi-logarithmic plane $K_1 > 0$: —, transition boundary from spatiotemporal chaos (SpC) to cluster synchronization (ClS); (——), transition boundary from cluster synchronization to stable synchronization (SS). The parameters used are those in Fig. 5.

When each chaotic electromechanical system of the network is coupled to another exclusively through a capacitor Fig. 6(a) presents $\Lambda(N, K_1)$'s variations and Fig. 6(b) the corresponding stability map in the parametric plane (N, K_1).We can toughly distinguish two domains in that plane.

Firstly, one has the *stable synchronization (SS) domain* in which $\Lambda<0$, i.e. all the conditional Lyapunov exponents are negative and the network of coupled chaotic electromechanical systems is assumed to synchronize. It comes out from these figures that the minimal value of K_1 above which there is stable synchronization domains increases as the number of electromechanical systems increases. This result is confirmed by the numerical simulation of Eq. (9) whose results are reported on the same map. A similar result has been established in Ref. [14] for a ring of diffusively coupled Duffing oscillators and in Ref. [17] for a ring of coupled Van der Pol oscillators. Let us focus in Fig. 6(b) to note that direct numerical simulations of Eq. (9) reveal the presence of an area where no synchronization is possible within SS area. The analysis of Λ's behaviour (Fig. 6(a)) through the stable domain reveals the existence of a peak where the width is spread out in this no synchronization sub-domain. This peak of Λ can be understood by the presence of the possible parametric resonances in the variational equations. This aspect revealed by the numerical procedure indicates that the synchronization stability condition does not always guarantee the realization of synchronous states. Indeed when $\Lambda \to 0^-$ (i.e. in the stable domain, near the stability threshold or where Λ displays a marked peak), synchronous states are weakly stable. Two situations can be observed during numerical simulations: Firstly,

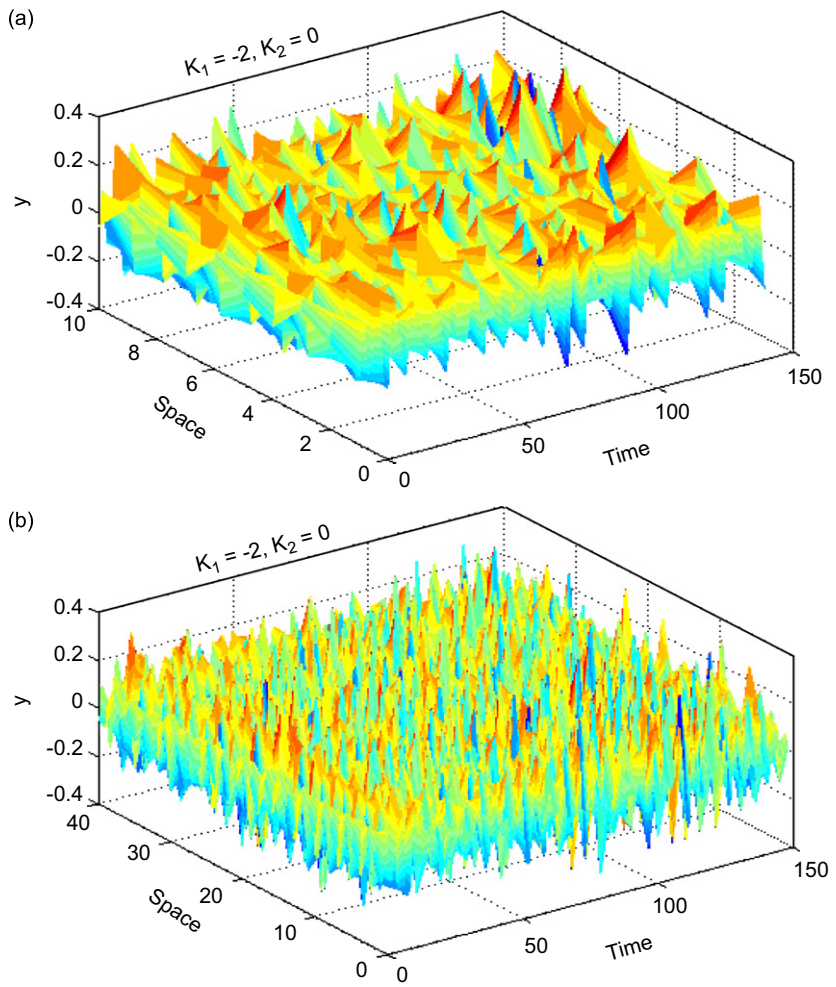

Fig. 8. Space–time–amplitude plot showing instability (unstable synchronization) in the network of diffusively coupled oscillators. The parameters used are those in Fig. 5.

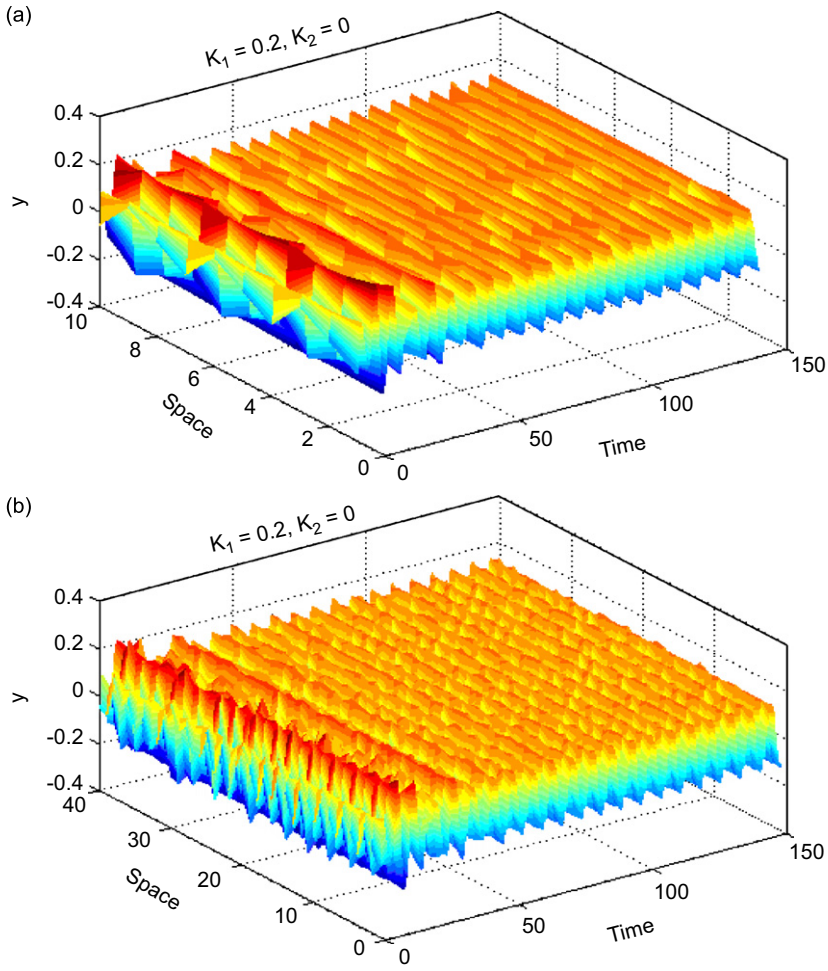

Fig. 9. Space–time–amplitude plot showing spatiotemporal chaos in the network (unstable synchronization). The parameters used are those in Fig. 5. Y is the amplitude of the linear mechanical oscillators.

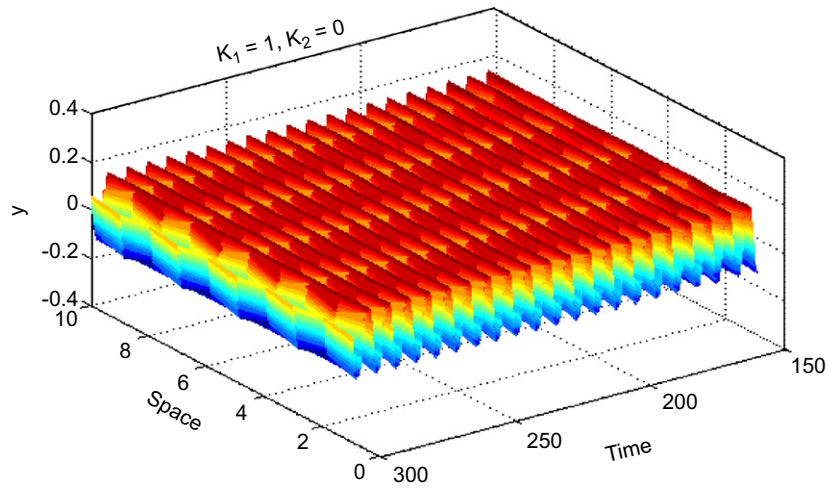

Fig. 10. Space–time–amplitude plot showing cluster synchronization in the network (unstable synchronization). In this case, particles whose positions in the site have the same parity behave in the same fashion. The parameters used are those in Fig. 5.

an intermittent synchronization is observed, which ends up giving place to sustainable chaos when time evolves and secondly, synchronization is achieved just after large transitory time, owing to the parametric resonance, such that one may practically consider that there is no synchronization. This is characterized by a very slow temporal decrease of transverse variations.

Secondly, we consider the *unstable synchronization (US) domain* in which $\Lambda \geqslant 0$, i.e. where at least one conditional Lyapunov exponent is positive. In the US area, according to the transverse eigenmodes distribution (in terms of stability) as K_1 varies, two different dynamical states can develop themselves in the network. If certain transverse modes are stable while other ones are unstable ($\lambda_k < 0$, for some values of k), we are in the clusters synchronization stability sub-domain. If all these modes are unstable ($\lambda_k > 0$, $\forall k$), we are in the spatiotemporal chaos sub-domain. We have represented the transition boundary, defined by $\lambda_k^{\min} = 0$, $k = 1, \ldots, N-1$, between these two dynamical states in Fig. 7 for $K_1 > 0$. This figure is just a version of Fig. 6(b), where the white zone included in the SS area is where, numerically, synchronization is not achieved. The change of concavity is due to the logarithmic scale used. To facilitate the readability, we chose a

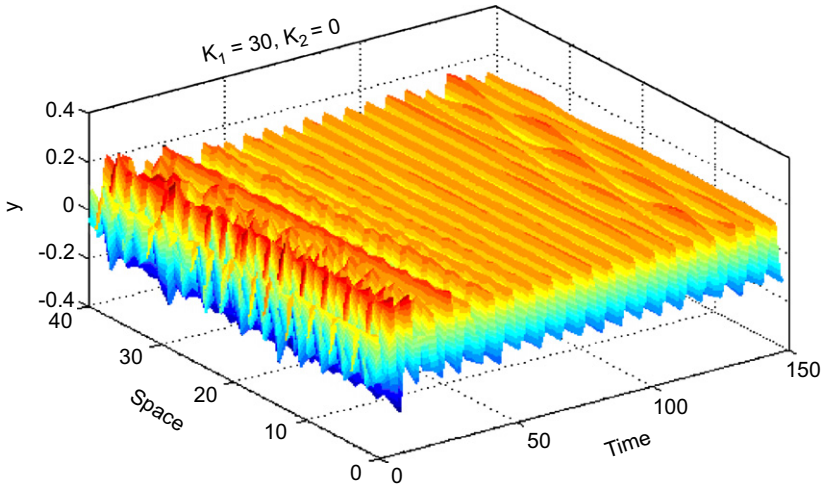

Fig. 11. Space–time–amplitude plot showing spatiotemporal chaos in stable clusters synchronization area. The parameters used are those in Fig. 5. Y is the amplitude of the linear mechanical oscillators.

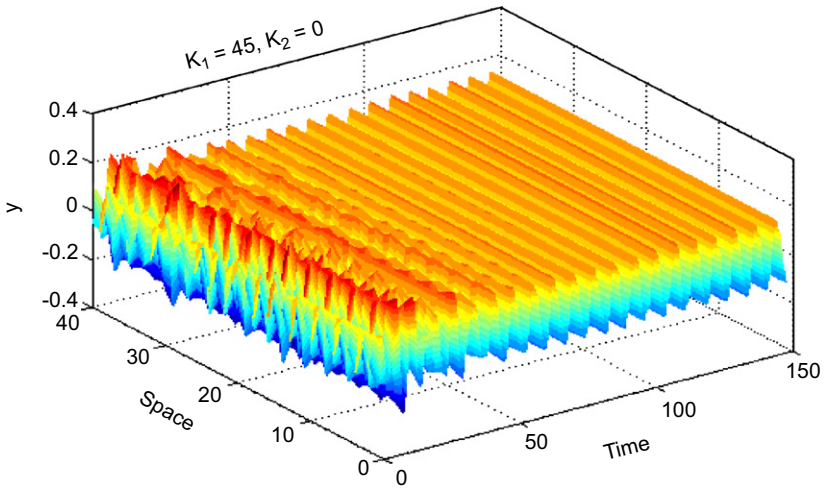

Fig. 12. Space–time–amplitude plot showing complete synchronization in the network (stable synchronization). The parameters used are those in Fig. 5. Y is the amplitude of the linear mechanical oscillators.

logarithmic scale because spatiotemporal chaos appears in the network for very low values of the coefficient K_1. Indeed, in the weak-couplings limit, we expect that the motion of a single oscillator of the network is qualitatively similar to that of an uncoupled oscillator under noise effect. The noisy motion of an uncoupled oscillator occurs on a slightly fuzzy version of the original attractor [28]. We must insist on the fact that cluster states are seldom observed during numerical simulations or in practice because of the weak stability of almost all the clusters so that they degenerate quickly into spatiotemporal chaos states [13,14,17]. In order to shed light on the numerical procedure results which confirm the dynamics of the system in each area evoked above, we represented the space–time–amplitude of the mechanical parts of the network for some parameter combinations.

Summing up what we have said above, for a fixed value of N, there are three main dynamical states that can develop in the network, according to the distribution of transverse modes through the Strutt diagram [14]. For relatively large negative values of K_1, $\Lambda \to \infty$ (i.e. certain transverse deviations infinitely move away from attractor S). This is the sign of a strong instability which shows up because of the wildly disordered nature of the spatiotemporal dynamics of the network (Fig. 8). For weak coupling values ($|K_1| < 1$), all the transverse Lyapunov exponents are positive, but all the transverse deviations are bounded. This shows up in Fig. 9 by the less spatially disordered behaviour of the network. In the sub-domain of stable clusters synchronization, some

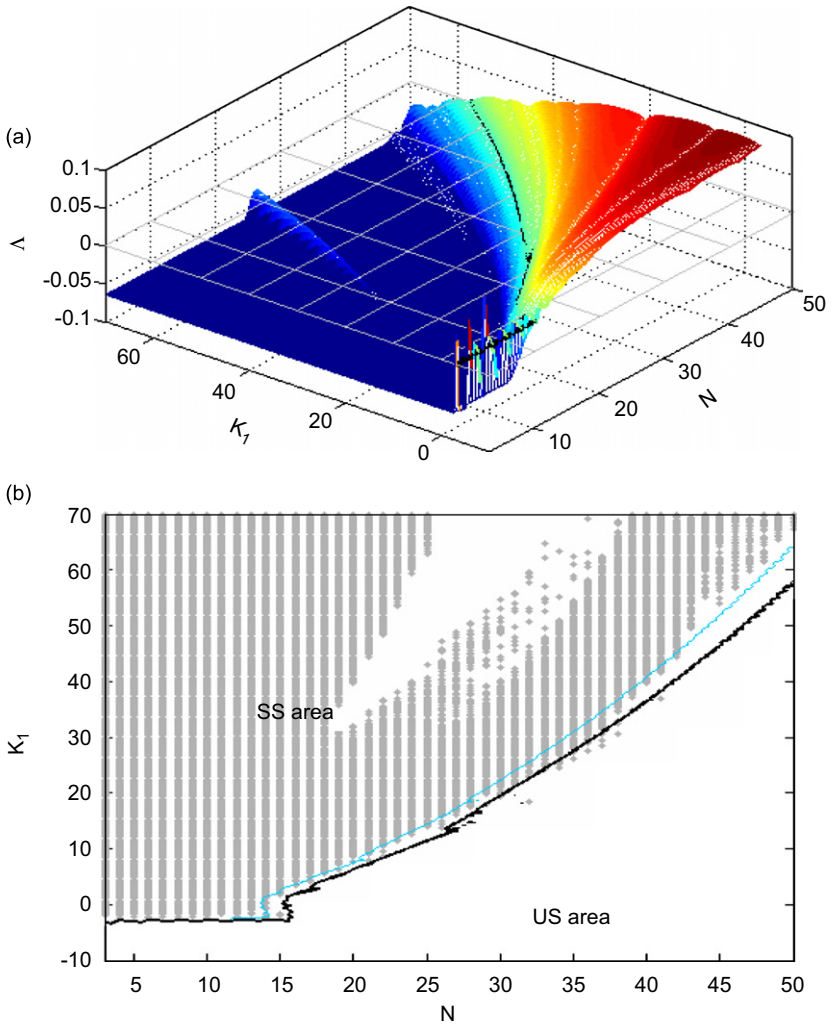

Fig. 13. (a) The MSF in the parametric plane (N, K_1). (b) The corresponding stability map: (——), stability threshold $\Lambda = 0$; same comments as at Fig. 6. For $K_2 = 1$, and the other parameters are those in Fig. 5.

scarce clusters are carried out and remained stable like it appeared in Fig. 10, the majority of these scarce clusters degenerate into spatiotemporal chaos regime (see Fig. 11 for $N = 40$ and K_1 chosen near the stability boundary). For relatively large values of the coupling, one enters into the stable synchronization domain as shown in Fig. 12. The stability diagram of Fig. 6(b) shows that the numerical threshold rather seems to be confused with the isoclines $\Lambda = -0.02$, but one can note that the MSF approach truly makes it possible to approximate the numerical border and to predict local instabilities capable of occurring in the SS area.

4.1.2. Dispersive–dissipative coupling case, i.e. $K_2 \neq 0$

Figs. 13 and 14 show that when K_2 grows, Λ's peaks lessen progressively, causing the stability boundary of the synchronization to move away. The stabilizing virtues of K_2 are due to the nature of the corresponding coupling element. Indeed, K_2 is a dissipative coupling that consequently reinforces the exponential decay of the transverse perturbations. The numerical procedure confirms the semi-numerical results. One can observe on the diagrams the remoteness of the stability boundary and the progressive disappearance of the no synchronization sub-domain included in SS area of Fig. 6. In order to show the effect of the dissipative component of the coupling on the stability boundary of the synchronization process, we present in Fig. 15 the stability diagrams for two different values of N.

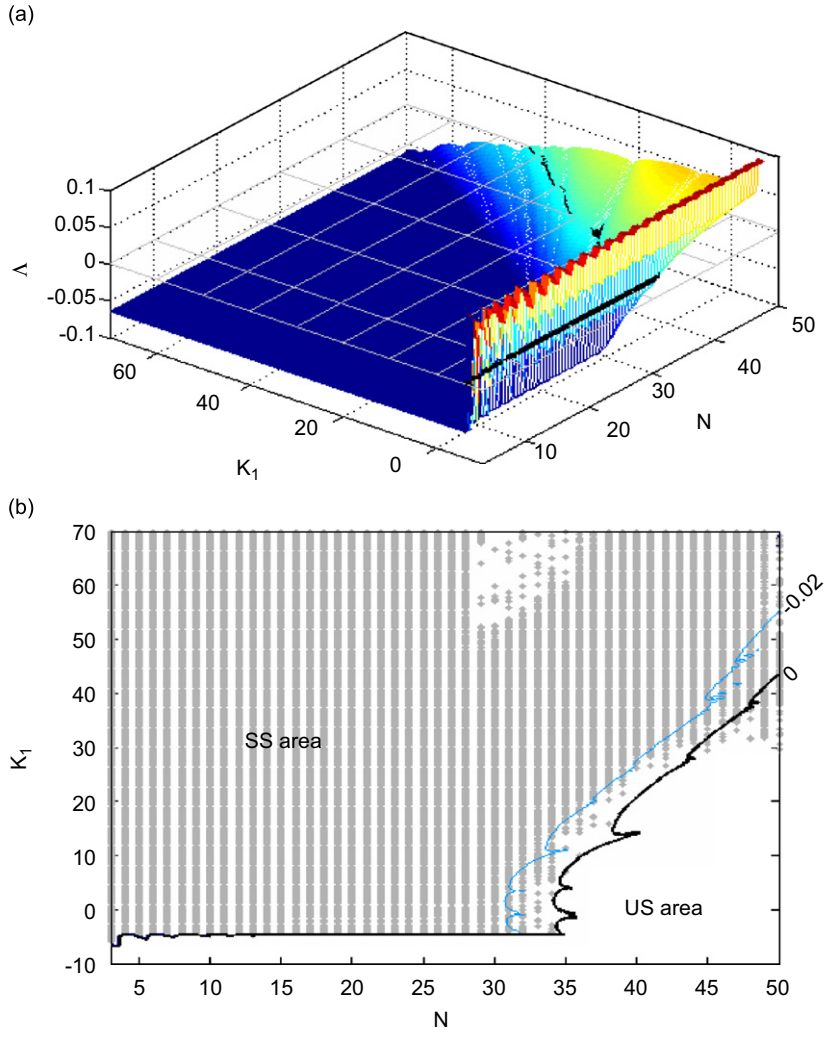

Fig. 14. (a) The MSF in the parametric plane (N, K_1). (b) The corresponding stability map: (——), stability threshold $\Lambda = 0$; same comments as in Fig. 6. For $K_2 = 5$, and the other parameters are those in Fig. 5.

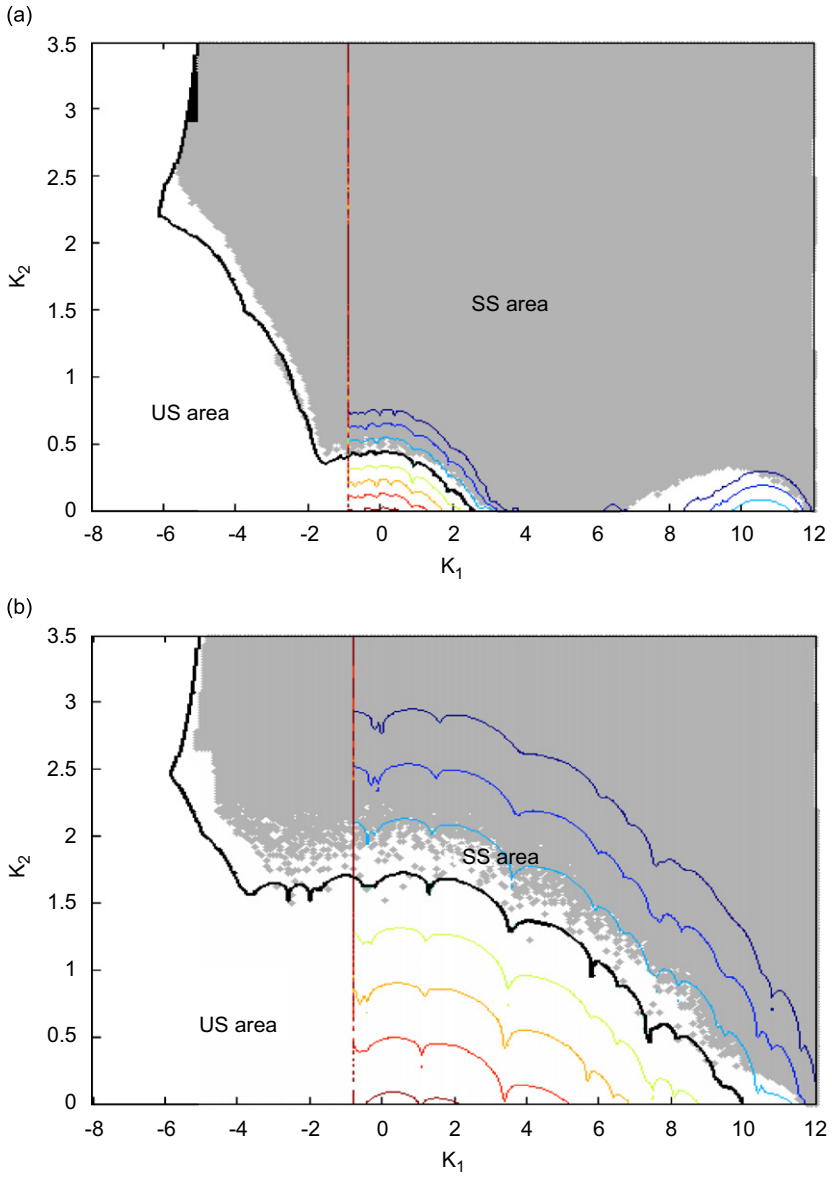

Fig. 15. The MSF contours and the corresponding stability map in the parametric plane (K_1, K_2): (——), stability threshold $\Lambda = 0$; the line displays the isoline $\Lambda = -0.02$, the dark domain is the complete synchronization area (obtained numerically). (a) $N = 10$ and (b) $N = 20$. The parameters used are those in Fig. 5.

4.2. The all-to-all coupling configuration

For the global coupling configuration, we also begin by considering the dispersive coupling configuration before analysing the effects of the dissipative coupling coefficient. For this purpose, we consider first $Q_2 = 0$, and determine in Fig. 16 some Λ's contours and the corresponding stability map in the (N, Q_1) plane. Unlike in the nearest-neighbour coupling configuration, the stable synchronization domain increases when N increases. We remember that for the nearest-neighbour coupling configuration, the number of transverse modes is an increasing function of N; consequently, increasingly large values of Q_1 will be necessary to overcome instabilities generated by the new eigenmodes [14,17]. In the all-to-all coupling configuration, all the

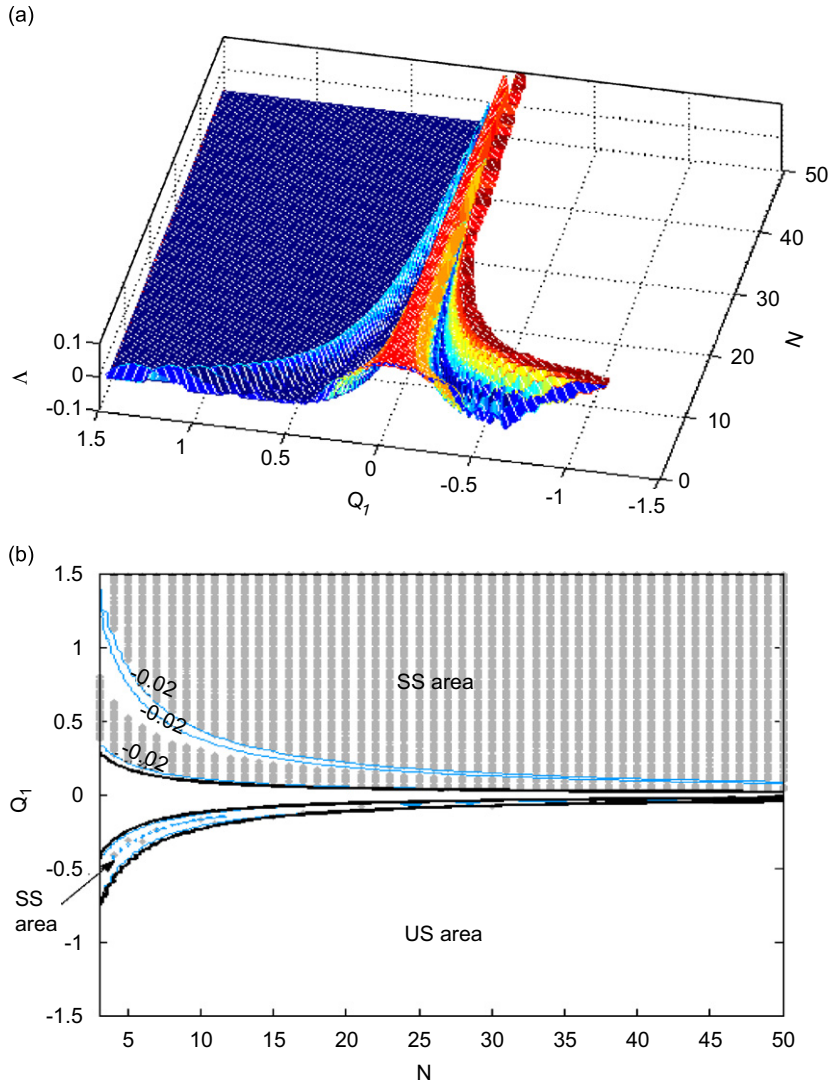

Fig. 16. (a) The MSF in the parametric plane (N, Q_1). (b) The corresponding stability: (——), stability threshold $\Lambda = 0$; the line displays the isoline $\Lambda = -0.02$, the dark domain is the complete synchronization area (obtained numerically). For $Q_2 = 0$ and the other parameters are those in Fig. 5.

transverse modes degenerate into only one. Therefore, in this case, the increase in the number of oscillators reinforces the coupling between all the oscillators (the addition of an oscillator in an N-network generates N new links) without, however, increasing the number of transverse modes. In this case, we find theoretically that the network of electromechanical systems will be able to exhibit only two main dynamical states; namely spatiotemporal chaos when the degenerated eigenmode is unstable and complete synchronization when this mode is stable.

The MSF's behaviour (see Fig. 16(a)) once more enables us to explain the presence of the no synchronization sub-domain appearing in the stable synchronization domain of Fig. 16(b). According to this figure, Λ admits a peak whose width is spread out in this sub-domain.

The dissipative component Q_2 of the coupling makes therefore a stronger demonstration of its stabilizing virtues. In fact, even for just $Q_2 = 0.02$ and $N \geqslant 10$, one notes in Fig. 17 that the unstable domain centred around the line $Q_1 = 0$ of Fig. 16 completely disappears, that the no synchronization sub-domain included in

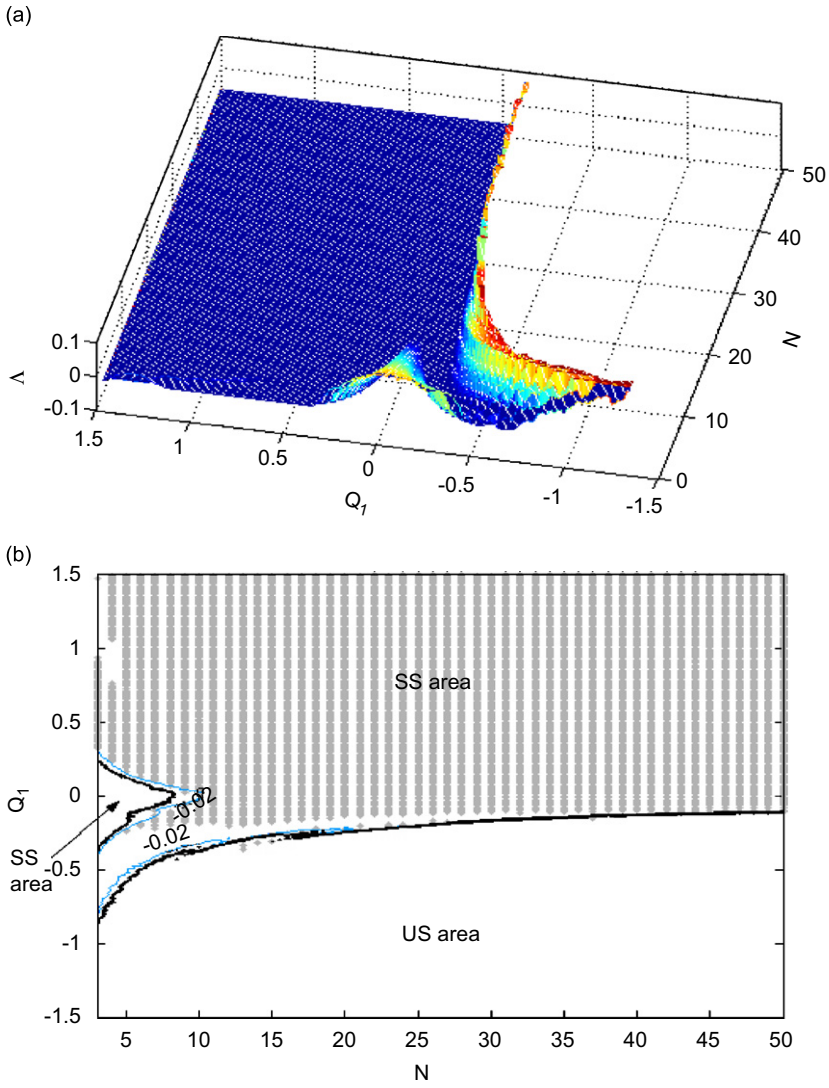

Fig. 17. (a) The MSF in the parametric plane (N, Q_1). (b) The corresponding stability: (——), stability threshold $\Lambda = 0$; the line displays the isoline $\Lambda = -0.02$, the dark domain is the complete synchronization area (obtained numerically). For $Q_2 = 0.02$, and the other parameters are those in Fig. 5.

the SS area also disappears, and that the lowest stability boundary is pushed away leading to an increase in the SS area. It remains to note that this boundary moves away from the boundary of the dispersive case, but ends up being stabilized for relatively large values of Q_2 (see Fig. 18).

In a general way, we can notice a good correspondence between the MSF approach results and those of the direct numerical simulations of Eqs. (9) and (14). Before starting with the conclusion, it must be noticed that the cases where K_1 or Q_1 are negative constitute a mathematical speculation, owing to the fact that the capacitance of a capacitor cannot be negative. However, these cases have also been treated, because the equations of the network (Eqs. (9) and (14)) can be models for other physical systems.

5. Conclusion

We have studied in this paper the stability of the synchronization states in the network of a shift-invariant set of N (nearest-neighbour or all-to-all) mutually coupled Duffing-quintic electromechanical transducers. The

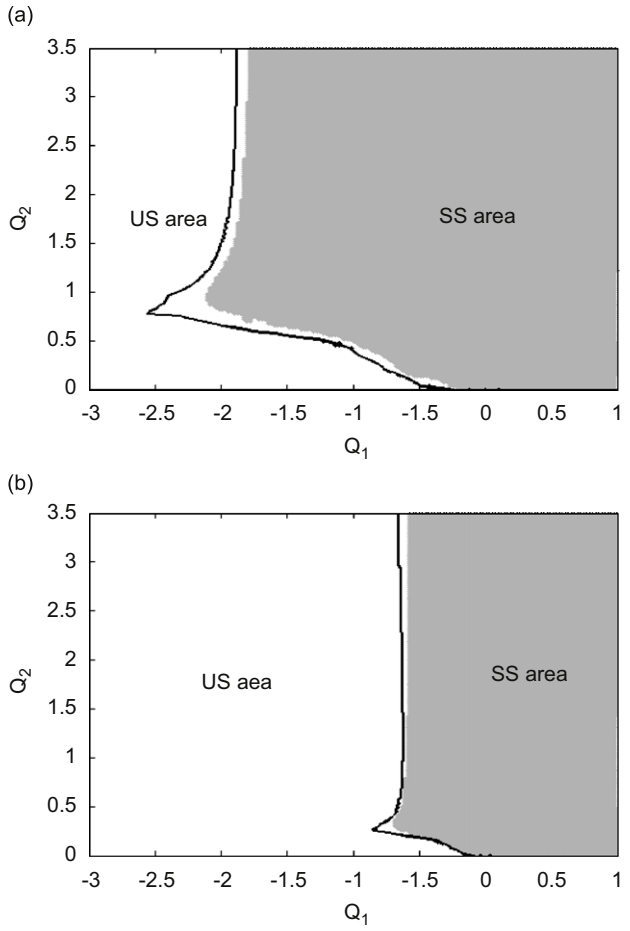

Fig. 18. The stability map in the parametric plane (Q_1, Q_2): (——), stability threshold $\Lambda = 0$, the dark domain is the complete synchronization area (obtained numerically). (a) $N = 10$ and (b) $N = 30$. The parameters used are those in Fig. 5.

MSF approach has shown to be powerful in the study of the stability of the synchronization process and consequently in the determination of the coupling strengths range which give place to certain synchronous states. A general analysis of the synchronization stability has played a key role in the determination of the potential conditions of realization of clusters and spatiotemporal chaos. This method has been necessary to shed light on the explanation of the de-synchronization phenomena that occur in stable synchronization areas. Numerical procedures have confirmed the semi-numerical results of the analytical method. These results revealed the importance of the association of the two coupling elements. Indeed, the dissipative component of the coupling (the resistance) optimizes the synchronization by reducing the time necessary for the implementation of this process.

The study has mainly focussed on analytical and numerical investigations. We think that an extension of the analytic treatment to find stability of synchronous states in the network of non-identical coupled chaotic electromechanical systems would be an interesting task, which can be tackled using Fourier analysis or a variation of the Kuramoto order parameter. Moreover, the spontaneous transition frequencies in the network with induced-noise can also be observed if one can resolve in time electronic circuits or through experimental investigations.

Acknowledgements

R. Yamapi undertook part of this work with the support of the International Centre for Theoretical Physics (ICTP) Programme for Training and Research in Italian Laboratories, Trieste, Italy. He also acknowledges

the support of the Laboratorio Regionale CNR/INFM, Dipartimenti di Fisica, Università di Salerno (Baronissi, Italy). P. Woafo acknowledges the support from the Humboldt Foundation and the Department of Nonlinear Dynamics, Max-Planck Institute for Dynamics and Self-Organisation (Gottingen, Germany). The authors thank Dr. Enjieu Kadji Hervé for fruitful suggestions.

References

[1] S. Boccaletti, J. Kurths, G. Osipov, D.L. Valladares, C.S. Zhou, The synchronization of chaotic systems, *Physics Reports* 366 (2002) 1–101.
[2] S. Boccaletti, V. Latora, Y. Moreno, M. Chavez, D.-U. Hwang, Complex networks: structure and dynamics, *Physics Reports* 424 (2006) 175–308.
[3] L.M. Pecora, T. Carroll, Master Stability Functions for synchronized coupled systems, *Physics Review Letters* 80 (10) (1998) 2109–2112.
[4] L.M. Pecora, Synchronization conditions and desynchronization patterns in coupled limit-cycle and chaotic systems, *Physical Review E* 58 (1) (1998) 347–360.
[5] M. Barahona, L.M. Pecora, Synchronization in small-world systems, *Physics Review Letters* 89 (2002) 054101.
[6] G. Hu, J. Yang, W. Liu, Instability and controllability of linearly coupled eigenvalue analysis oscillators, *Physical Review E* 58 (1998) 4440–4453.
[7] M. Zhan, G. Hu, J. Yang, Synchronization of chaos in coupled systems, *Physical Review E* 62 (2000) 2963–2966.
[8] M. Chen, D. Zhou, Synchronization in uncertain complex networks, *Chaos* 16 (013101) (2006) 1–8.
[9] K.S. Fink, G. Johnson, T. Carroll, D. Mar, L. Pecora, Three coupled oscillators as a universal probe of synchronization stability in coupled oscillator arrays, *Physical Review E* 61 (5) (2000) 5080–5090.
[10] S.E. de S. Pinto, S.R. Lopes, R.L. Viana, Collective behavior in a network of Van der Pol oscillators with power–law coupling, *Physica A* 303 (2002) 339–356.
[11] J.F. Heagy, T.L. Carroll, L.M. Pecora, Synchronous chaos in coupled oscillator systems, *Physical Review E* 50 (3) (1994) 1874–1885.
[12] L.M. Pecora, T.L. Carroll, Synchronization in chaotic systems, *Physics Review Letters* 64 (8) (1990) 821–824.
[13] Y. Zhang, G. Hu, H.A. Cerdeira, S. Cheng, T. Braun, Y. Yao, Partial synchronization and spontaneous spatial ordering in coupled chaotic systems, *Physical Review E* 63 (026211) (2001) 1–9.
[14] Y.C. Kouomou, P. Woafo, Transition from spatiotemporal chaos to cluster and complete synchronization states in a shift-invariant set of coupled nonlinear oscillators, *Physical Review E* 67 (046205) (2003) 1–8.
[15] Y.C. Kouomou, P. Woafo, Generalized correlated states in a ring of coupled nonlinear oscillators with a local injection, *Physical Review E* 66 (066201) (2002) 1–6.
[16] P. Woafo, H.G. Enjieu Kadji, Synchronized states in a ring of mutually coupled self-sustained electrical oscillators, *Physical Review E* 69 (046206) (2004) 1–8.
[17] H.G. Enjieu Kadji, J.B. Chabi Orou, P. Woafo, Spatiotemporal dynamics in a ring of N mutually coupled self-sustained systems, *Chaos* 17 (3) (2007) 033109.
[18] T. Endo, S. Mori, Mode analysis of a ring of large number of mutually coupled Van der Pol oscillators, *IEEE Transactions Circuits Systems* 25 (1) (1978) 7–18.
[19] P. Woafo, Transitions to chaos and synchronization in a nonlinear emitter–receiver system, *Physics Letters A* 267 (2000) 31–39.
[20] H. Gang, X. Jinghua, G. Jihua, L. Xiangming, Y. Yugui, B. Hu, Analytical study of spatiotemporal chaos control by applying local injections, *Physical Review E* 62 (3) (2000) 3043–3046.
[21] R. Yamapi, Synchronization dynamics in a ring of four mutually inertia coupled self-sustained electrical systems, *Physica A* 366 (2006) 187–196.
[22] R. Yamapi, S. Bocalletti, Active control of the synchronization manifold in a ring of mutually coupled oscillators, *Physics Letters A* 371 (2007) 48–57.
[23] R. Yamapi, P. Woafo, Synchronized states in a ring of four mutually coupled self-sustained electromechanical devices, *Communication in Nonlinear Sciences and Numerical Simulations* 11 (2006) 186–202.
[24] G.S.M. Ngueuteu, R. Yamapi, P. Woafo, Effects of higher nonlinearity on the dynamics and synchronization of two coupled electromechanical devices, *Communication in Nonlinear Sciences and Numerical Simulations* 13 (7) (2008) 1213–1240.
[25] V.Y. Taffoti Yolong, P. Woafo, Synchronization in a ring of mutually coupled electromechanical devices, *Physica Scripta* 74 (2006) 591–598.
[26] Y.C. Kouomou, P. Colet, N. Gastaud, L. Larger, Effect of parameter mismatch on the synchronization of chaotic semiconductor lasers with electro-optical feedback, *Physical Review E* 69 (056226) (2004) 1–15.
[27] V. Ahlers, U. Parlitz, W. Lauterborn, Hyperchaotic dynamics and synchronization of external-cavity semiconductor lasers, *Physical Review E* 58 (6) (1998) 7208–7213.
[28] D.K. Umberger, C. Grebogi, E. Ott, B. Afeyan, Spatiotemporal dynamics in a dispersively coupled network of nonlinear oscillators, *Physical Review A* 39 (9) (1989) 4835–4842.
[29] K. Miyakawa, K. Yamada, Synchronization and clustering in globally coupled salt-water oscillators, *Physica D* 151 (2001) 217–227.
[30] S. Nakata, T. Miyata, N. Ojima, K. Yoshikawa, Self-synchronization in coupled salt-water oscillators, *Physica D* 115 (1998) 313–320.